Electronic Supplementary Material (ESI) for Journal of Materials Chemistry A.

Vertically grown p-n heterojunction FeCoNi LDH/CuO arrays with modulated interfacial charges to facilitate electrocatalytic oxygen evolution reaction

Qi Ouyang[a], Shichao Cheng[a], Chunhui Yang[a], and Zuotao Lei*[a]

a MIIT Key Laboratory of Critical Materials Technology for New Energy Conversion and Storage, School of Chemistry and Chemical Engineering, Harbin Institute of Technology, Harbin, 150001, People's Republic of China

* Corresponding author: leizuotao@hit.edu.cn

1. Experimental section

1.1 Electrocatalysts preparation

All the agents are used directly without further purification.

1.1.1 Synthesis of $Cu(OH)_2$/Cu and CuO/Cu

Dropped 16 mL NaOH (10 M) slowly into 44 mL $(NH_4)_2S_2O_8$ (0.18 M) and kept stirring until the solution was clear and transparent. The Cu foam was cut into 6×6 cm^2 pieces and cleaned by ultrasonic treatment in acetone, ethanol, and dilute hydrochloric acid for 5 min each. The clean Cu foam was immersed in the above-mentioned solution for 20 min and gradually turned blue. The resulting product was $Cu(OH)_2$/Cu. After being rinsed clean by deionized water and dried overnight, $Cu(OH)_2$/Cu was subsequently calcined for 4 h in a muff furnace at 150 ℃ in the air with a slow heating rate of 1 ℃ min^{-1}. The product was CuO nanowires/Cu. When not specified, all the CuO/Cu mentioned in the manuscript are CuO nanowires/Cu.

1.1.2 Synthesis of CuO film/Cu and FeCoNi LDH+CuO/Cu

For comparison, CuO film/Cu and FeCoNi LDH+CuO/Cu were prepared. Since the Cu foam cannot be converted to CuO sufficiently after calcination at 150 ℃ for 4 h, the Cu foam was calcined at 300 °C for 3 h in air. The loading mass of CuO on CuO film/Cu (3.5 mg cm^{-2}) obtained in this experimental method was similar to that of CuO nanowires/Cu (3.7 mg cm^{-2}) obtained in step 1.1.1. FeCoNi LDH+CuO/Cu was synthesized in the same way as FeCoNi LDH/CuO/Cu, except that the CuO film/Cu was used as the working electrode. The obtained product was noted as FeCoNi LDH+CuO/Cu.

1.1.3 Synthesis of FeCoNi LDH/Cu

FeCoNi LDH/Cu was synthesized in the same way as FeCoNi LDH/CuO/Cu, except that the Cu foam was used directly as the working electrode. The obtained product was noted as FeCoNi LDH/Cu.

1.1.4 Synthesis of FeCoNi LDH/CuO/Cu with different ratio of metal elements

FeCoNi LDH/CuO/Cu with different ratios of metal elements were synthesized in the same way as FeCoNi LDH/CuO/Cu-600, except that the feeding ratios of the metal raw materials were different.

1.2 Characterization

The morphology of the catalyst was observed by scanning electron microscope (SEM, Zeiss Supra, 150 KV) and high-resolution transmission electron microscope (HRTEM, FEI Tecnai G2 F20). The phase of the catalyst was determined by powder X-ray diffraction (XRD, Bruker D8 Advance, Cu Kα, 1° min^{-1}). The elemental composition of the catalyst was determined by an inductively coupled plasma optical emission spectrometer (ICP-OES, Thermo, iCAP 7400). The thickness of the nanosheet was determined by atomic force microscopy (AFM, Bruker, Dimension Fastscan). X-ray photoelectron spectroscopy (XPS, Thermo Fisher Scientific, Escalab 250Xi, Al Kα) was employed to analyze the chemical environment of the elements. An Ultraviolet photoelectron spectrometer (UPS, PHI5000 VersaProbe III) was used to determine the work function and valence band of the sample. The bandgap of the sample was analyzed by the ultraviolet-visible diffuse reflectance spectrum (UV-vis DRS, Shimadzu, UV-3600Plus). Brunauer-Emmett-Teller (BET) method was used to calculat the specific

surface area on an automatic surface area and porosity analyzer (Micromeritics, TriStar II 3020).

1.3 Electrochemical measurements

All electrochemical tests were performed in a typical three-electrode system on an electrochemical workstation (Princeton Versa STAT). Oxygen-saturated KOH (1 M) solution was used as the electrolyte. The samples were cut into 1×1 cm^2 pieces and directly served as working electrodes. A graphite rod (d = 6 mm) and a Hg/HgO (1 M KOH) electrode were used as the counter electrode and reference electrode, respectively. For comparison, RuO_2/Cu electrode was made by coating the ink (3 mg RuO_2 mixed with 70 μL ethanol and 8 μL Nafion solution with adequate ultrasonic treatment) on a piece of Cu foam (1×1 cm^2). All electrochemical measurements were performed after 30 cycles of cyclic voltammetry (CV) test. The Mott-Schottky (M-S) plots were obtained with AC frequency of 3, 4, and 5 kHz under the same condition as OER measurements. The potentials were all calibrated to a reversible hydrogen electrode (RHE) using the following formula: $E_{\mathrm{RHE}} = E_{Hg/HgO\ (1\ \mathrm{M\ KOH})} + 0.098 + 0.0591 * p\mathrm{H}$. The linear sweep voltammetry (LSV) curves were obtained at a scan rate of 5 mV s^{-1} with iR correction. The TOF values were calculated by the following equation: TOF (s^{-1}) = ($|j| \times$ A) / (n × F × m). j (A cm^{-2}) is the current density. A is the geometric surface area of the electrode, and for all the sample A is 1 cm^2 in this manuscript. n is the number of electrons transferred in OER (n = 4). F is the Faraday constant. m (mol) is the mole number of all the transition metals atoms (including Fe, Co, Ni, and Cu) loaded on the Cu foam. The

molar ratio of Fe, Co, Ni in FeCoNi LDH was determined by ICP-OES. The comparasion of electrochemical surface areas (ECSA) was estimated by comparing the values of double-layer capacitance (C_{dl}), which were obtained by CV measurements with scan rates of 30, 40, 50, 60, 70 mV s^{-1} in the non-Faraday region. The electrochemical impedance spectroscopy (EIS) tests were carried out with the frequency ranging from 10k Hz to 0.1 Hz at the potential of 1.5 V (vs. RHE). The OH diffusion coefficient (D_{OH}) were obtained by CV measurements from 0.9 V to 1.7 V (vs. RHE) with scan rates of 1, 5, 10, 15, 20, 25, 30 mV s^{-1} based on the Sevick equation: $Jp = 2.65 \times 10^5 \times n^{3/2} \times A \times D^{1/2} \times C_0 \times v^{1/2}$, where Jp is the cathodic peak current, n is the number of transferred electrons, A is the surface area, D is the D_{OH}, C_0 is the concentration of OH and v is the scan rate. When n, A, and C_0 are constant, D_{OH} can be represented by the slope obtained by plotting Jp vs. $v^{1/2}$.[1, 2] The long-time stabilities of the sample at different potentials were evaluated by chronoamperometry measurements.

1.4 Density functional theory calculations

The Vienna Ab initio Package (VASP)[3, 4] was employed to perform all the density functional theory (DFT) calculations. The generalized gradient approximation (GGA) with the Perdew−Buker−Ernzerhof (PBE)[5] functional was adopted. The projected augmented wave (PAW) potentials[6, 7] were chosen to describe the core-electron interactions and take valence electrons into account using a plane-wave basis set with a kinetic energy cutoff of 450 eV. Partial occupancies of the Kohn-Sham orbitals were allowed using the Gaussian smearing method and a width of 0.02 eV. The electronic

energy was considered self-consistent when the energy change was smaller than 10^{-5} eV. Geometry optimization was considered convergent when the force change was smaller than 0.05eV/Å. Grimme's DFT-D3 methodology[8] was used to describe the dispersion interactions. The vacuum spacing in a direction perpendicular to the plane of the structure was 18 Å. The Brillouin zone integration was performed using 2×2×1 (FeCoNi LDH), 5×5×1 (CuO), and 1×1×1 (FeCoNi LDH /CuO) Monkhorst-Pack *k*-point sampling for a structure with a separation of 0.03 $Å^{-1}$. The free energy was calculated using the equation: $G = E + ZPE - TS$, in which G, E, ZPE, and TS were the free energy, total energy, zero-point energy, and entropic contributions from DFT calculations, respectively. The Hubbard U correction had been set as 3.75, 3.05, 4.13, and 2.96 eV for Ni, Co, Fe, and Cu atoms.

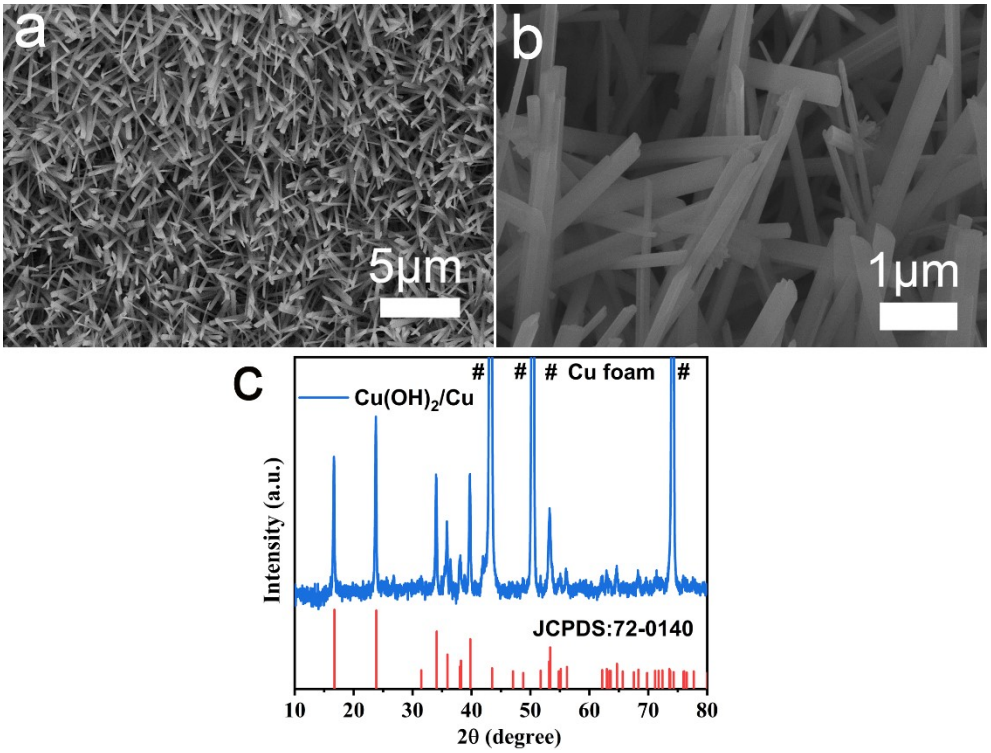

Fig. S1 (a-b) SEM images and (c) XRD pattern of $Cu(OH)_2/Cu$.

Since the published literature has confirmed that the catalytic performance of CuO nanowires is superior to that of CuO without specific morphology, the calcination temperature should be as low as possible to ensure complete conversion of $Cu(OH)_2$ to CuO but prevent excessive oxidation of the Cu substrate. Because the oxidation of Cu substrate increases the mass loading of CuO with no specific morphology.[1] XRD pattern (Fig. S2c) of the sample after calcination at 150 °C is attributed to CuO, indicating the complete conversion of $Cu(OH)_2$ to CuO. When calcined below this temperature, $Cu(OH)_2$ cannot be completely converted to CuO (Figs. S2d). Therefore, 150 °C is determined to be the optimal annealing temperature.

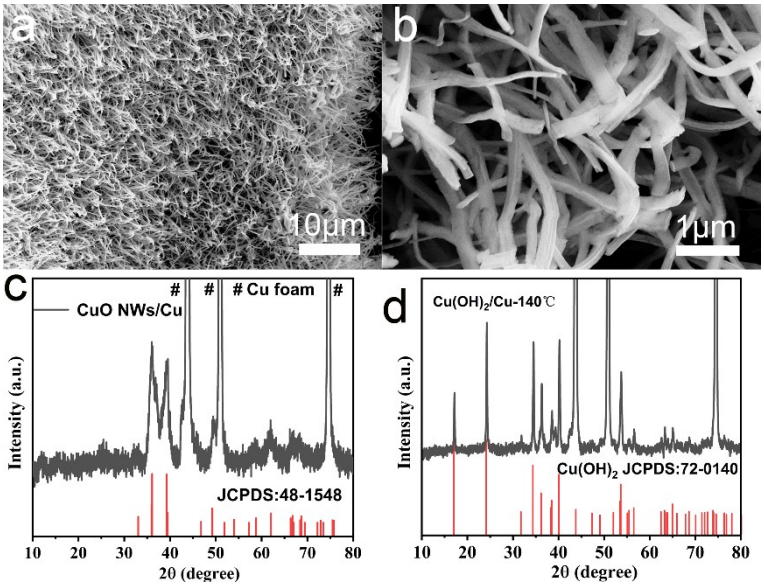

Fig. S2 (a-b) SEM images and (c) XRD pattern of CuO/Cu; (d) XRD pattern of $Cu(OH)_2$/Cu after calcination at 140°C.

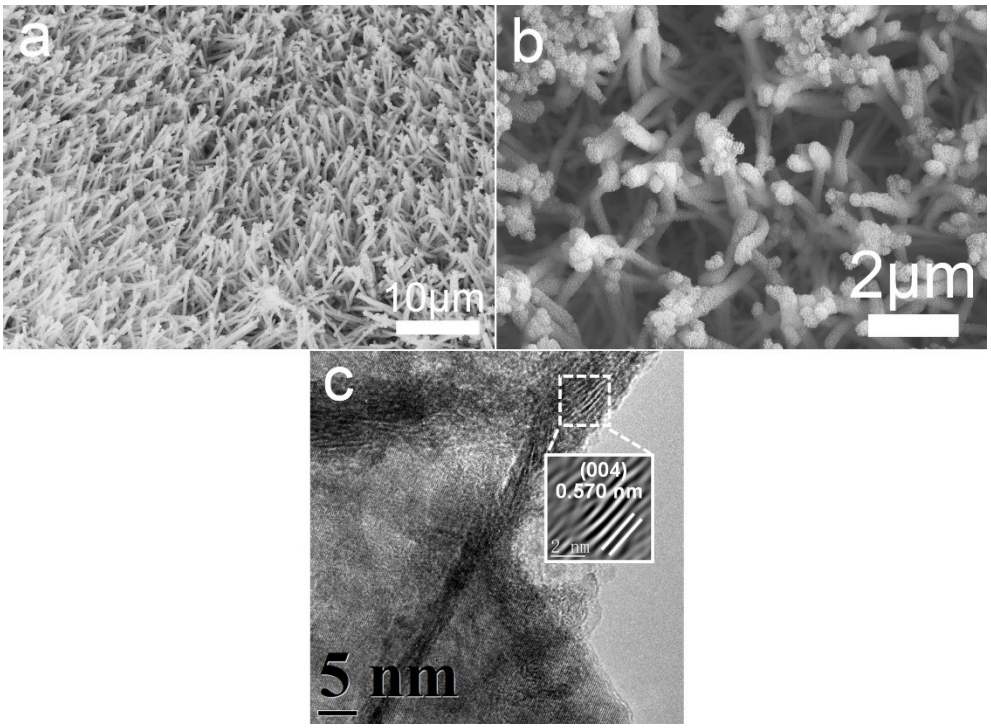

Fig. S3 (a-b) SEM images of FeCoNi LDH/CuO/Cu and (c) HRTEM image of FeCoNi LDH in FeCoNi LDH/CuO/Cu.

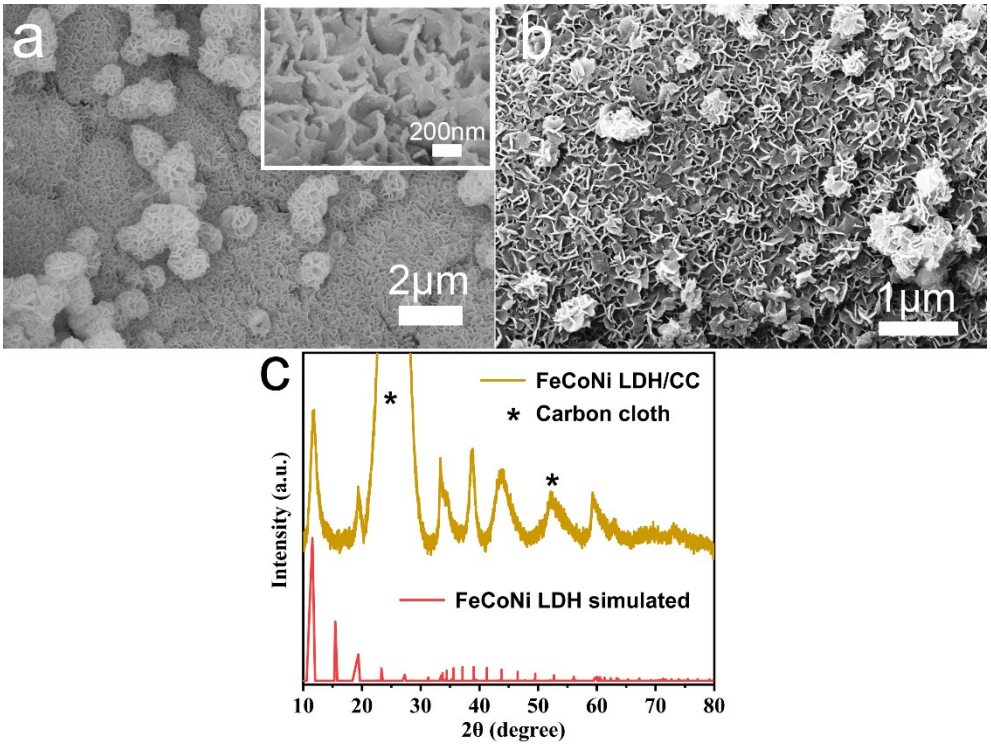

Fig. S4 (a) SEM images of FeCoNi LDH/Cu; (b) SEM image and (c) XRD pattern of FeCoNi LDH/CC. Since the intensity of the peaks attributed to Cu foam in the XRD pattern of FeCoNi LDH/Cu is too strong, making the peaks attributed to FeCoNi LDH not easily discernible, FeCoNi LDH/CC was prepared under the same experimental conditions to obtain a clearer XRD pattern.

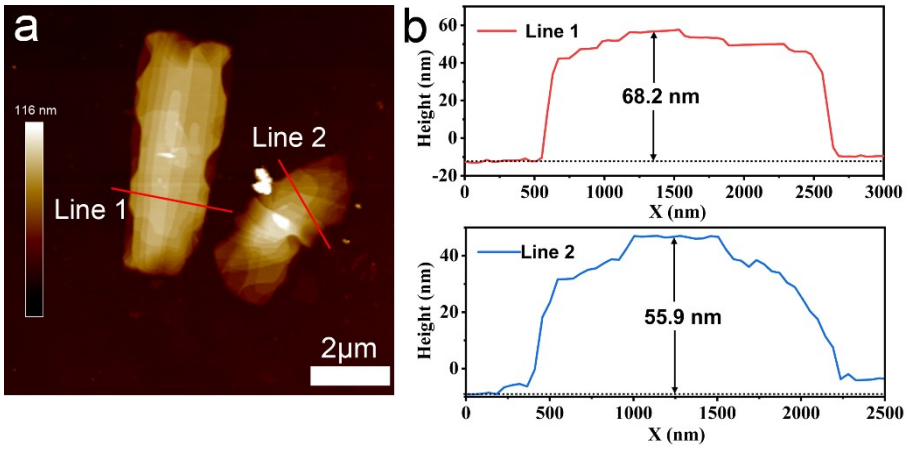

Fig. S5 (a) AFM image and (b) the corresponding height profiles of FeCoNi LDH nanosheets on FeCoNi LDH/Cu sample across line 1 and line 2 in (a).

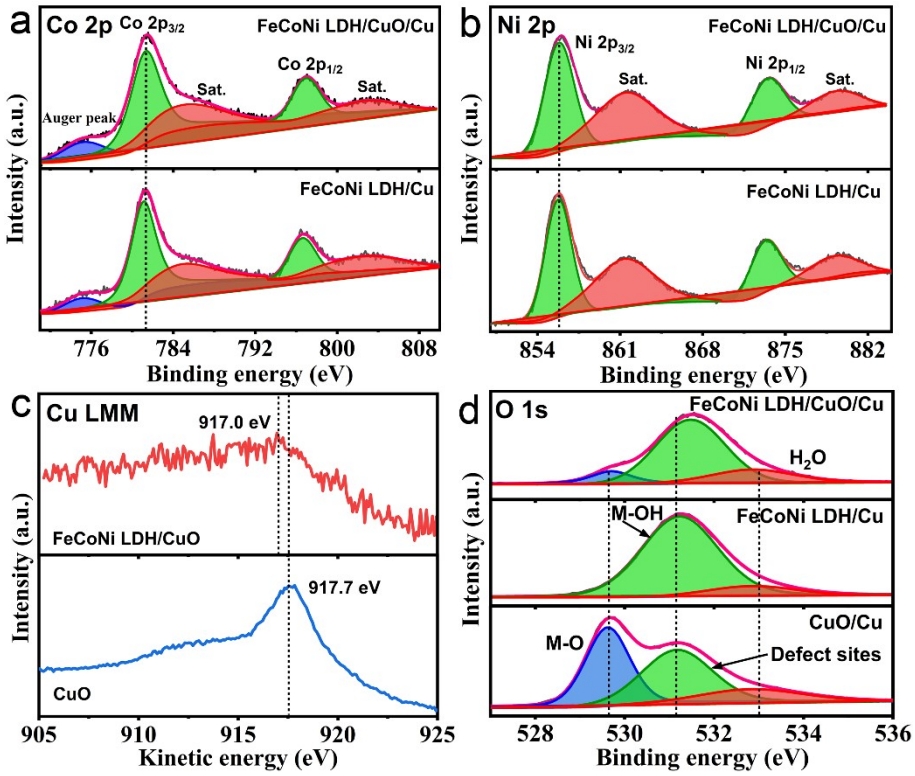

Fig. S6 High-resolution XPS spectra of (a) Co 2p, (b) Ni 2p, (c) Cu LMM and (d) O 1s.

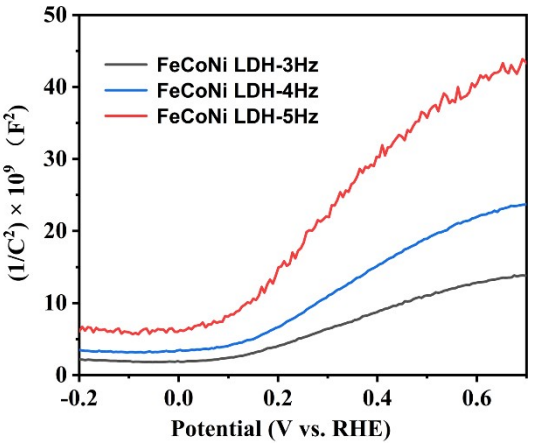

Fig S7 Mott-Schottky plots of FeCoNi LDH.

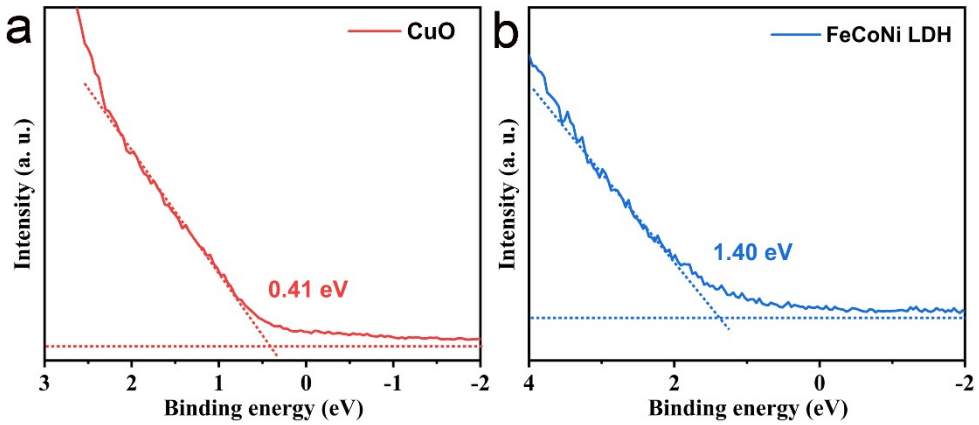

Fig. S8 UPS valence band spectra of (a) CuO and (b) FeCoNi LDH. The value of the intersection of the tangent line and the abscissa is the difference between the valence band and the Fermi level.

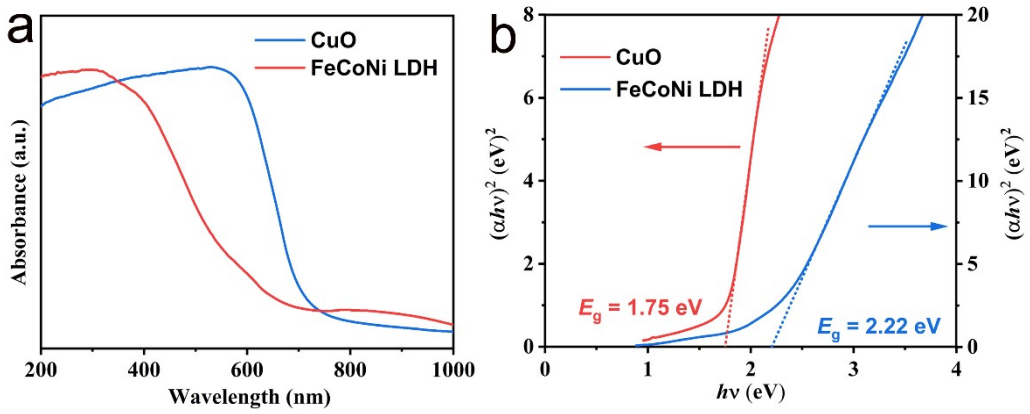

Fig. S9 (a) UV-vis diffuse spectra and (b) the corresponding Tauc plots of CuO and FeCoNi LDH.

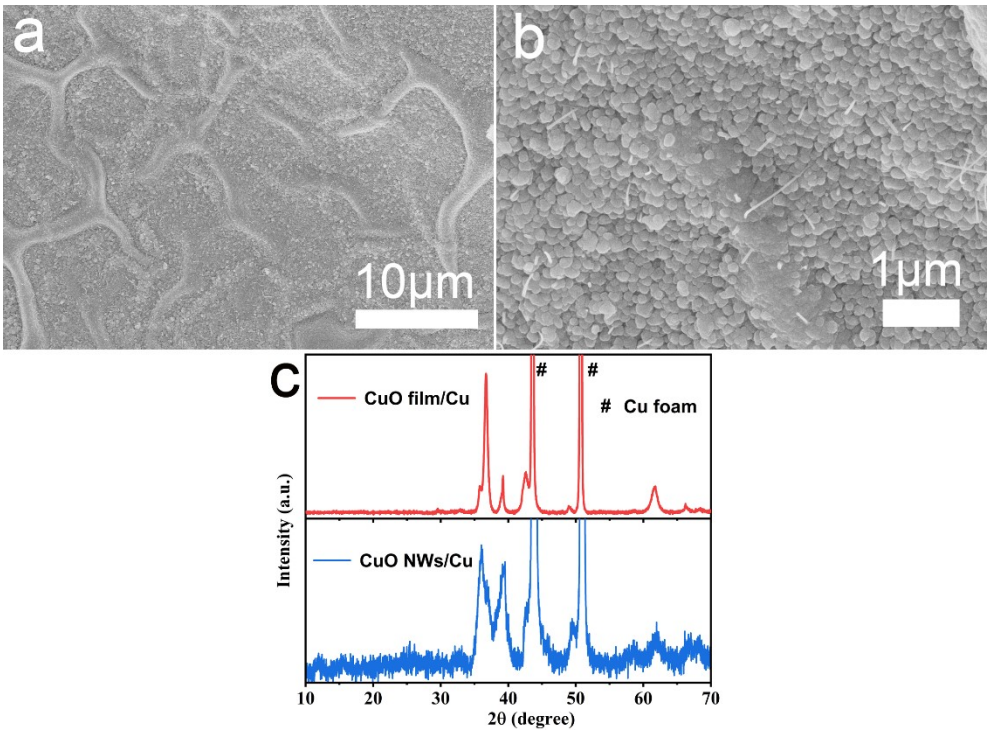

Fig. S10 (a-b) SEM images of CuO film/Cu; (c) XRD patterns of CuO film/Cu and CuO NWs/Cu.

Since the CuO film/Cu is obtained by calcination at a higher temperature, the characteristic peaks of CuO in its XRD pattern are sharper and narrower, but the positions of the characteristic peaks do not change, confirming that the CuO film and CuO NWs are the same phases. The calcination temperature is increased to obtain CuO film/Cu because Cu foam cannot be converted directly to CuO at the same calcination temperature as $Cu(OH)_2$/Cu (150 ℃). The calcination temperature and time (300°C, 3h) are finalized because the loading of CuO film obtained at this experimental condition is similar to that of the CuO NWs.

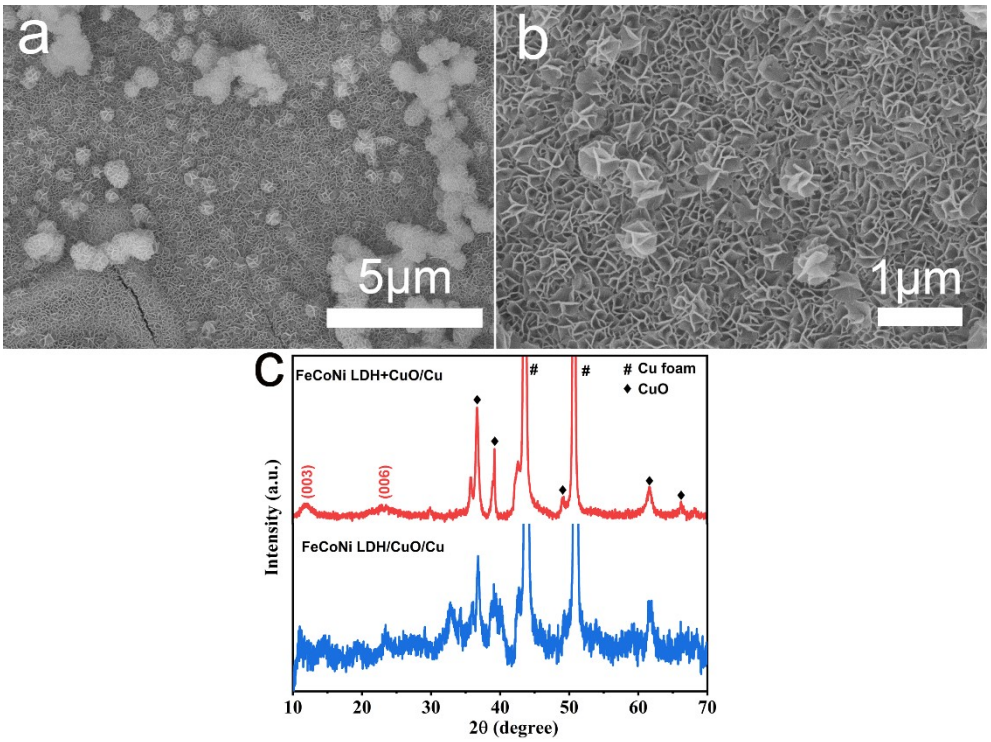

Fig. S11 (a-b) SEM images of FeCoNi LDH+CuO/Cu; (c) XRD patterns of FeCoNi LDH/CuO/Cu and FeCoNi LDH+CuO/Cu.

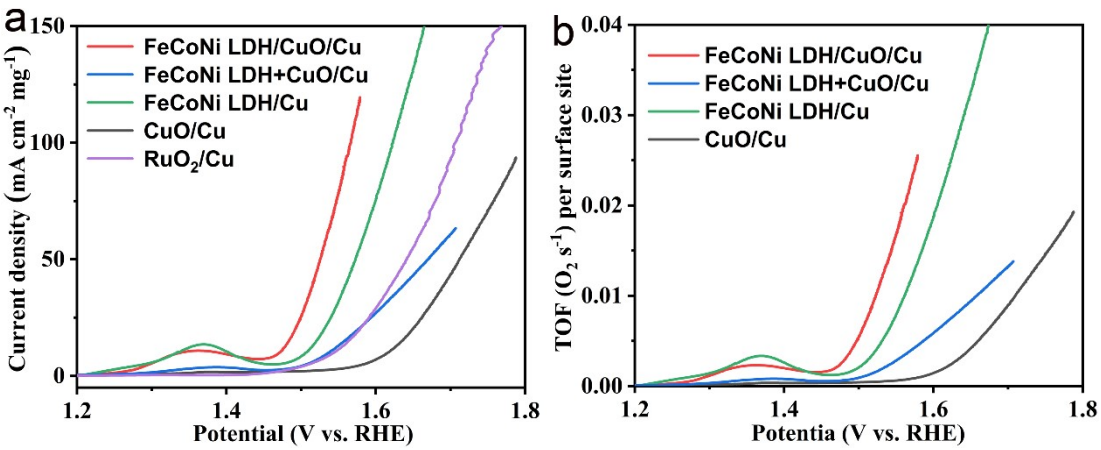

Fig. S12 (a) The mass activities and (b) TOF of the catalysts. The mass loadings of catalysts are shown in Table S1. The molar ratio of Fe, Co, Ni in FeCoNi LDH is determined by ICP-OES results (Table S2).

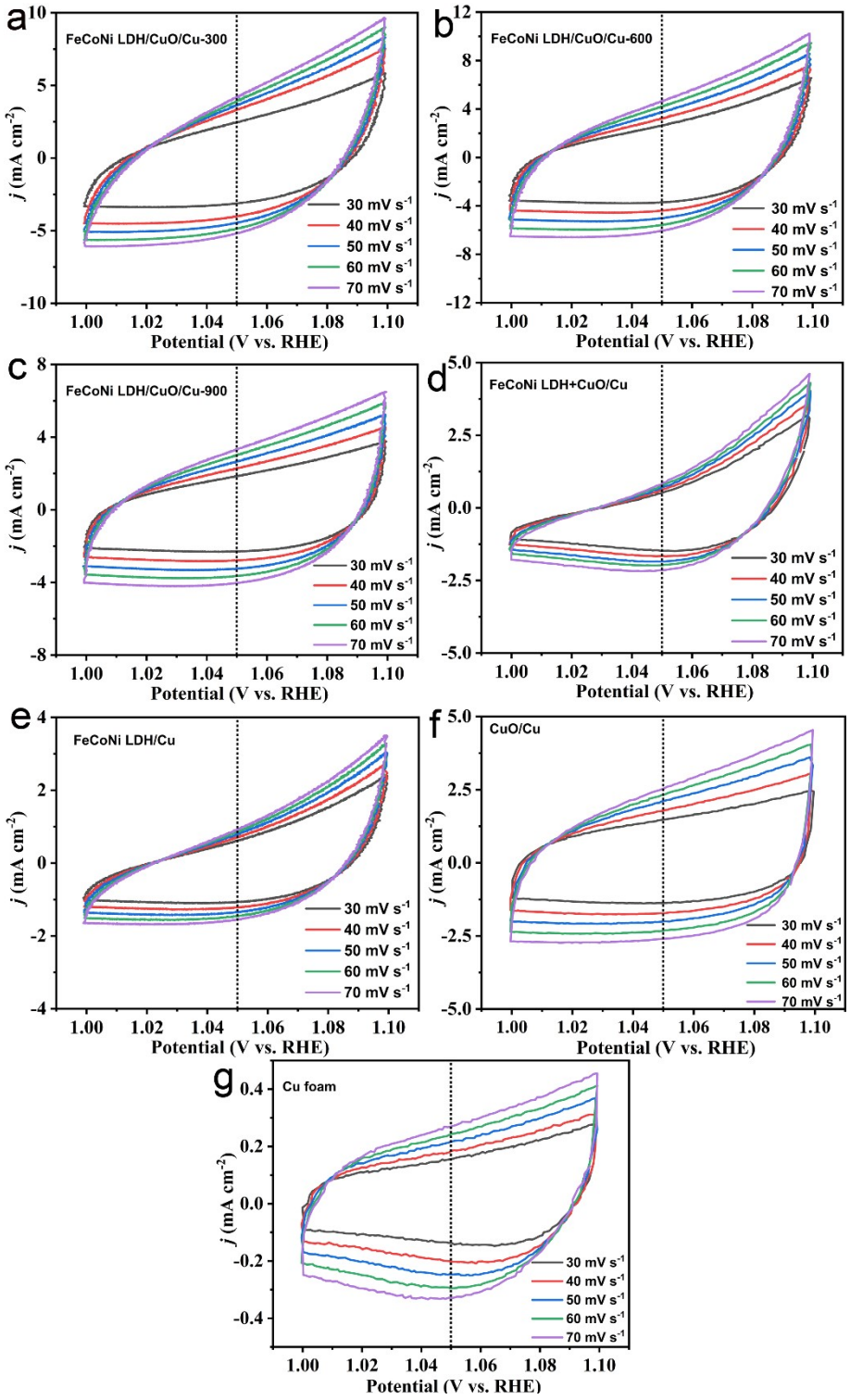

Fig. S13 CV curves of (a) FeCoNi LDH/CuO/Cu-300, (b) FeCoNi LDH/CuO/Cu-600, (c) FeCoNi LDH/CuO/Cu-900, (d) FeCoNi LDH+CuO/Cu, (e) FeCoNi LDH/Cu, (f) CuO/Cu and (g) bare Cu foam with different scan rates (30, 40, 50, 60, 70mV s^{-1}) from 1.00 V to 1.10 V (vs. RHE).

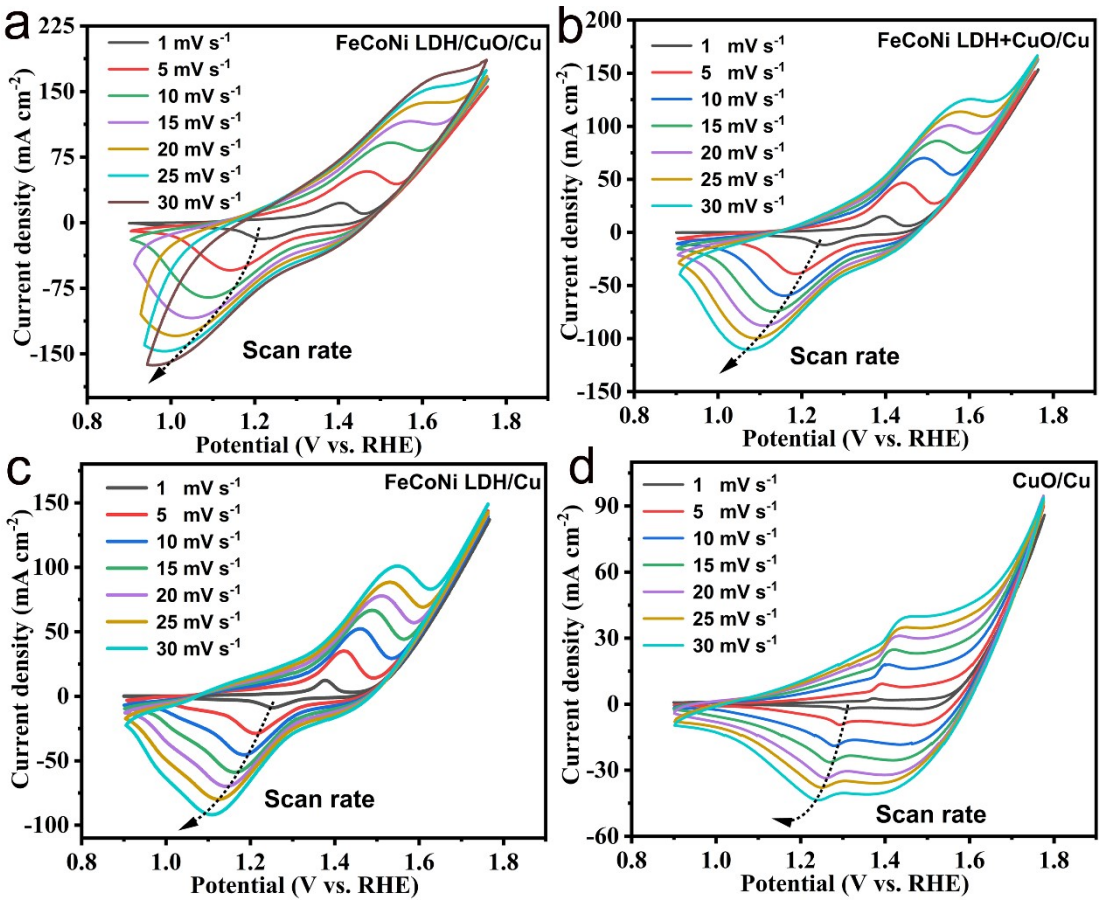

Fig. S14 CV curves of (a) FeCoNi LDH/CuO/Cu, (b) FeCoNi LDH+CuO/Cu, (c) FeCoNi LDH/Cu and (d) CuO/Cu with different scan rates (1, 5, 10, 15, 20, 25, 30 mV s^{-1}) from 0.90 V to 1.70 V (vs. RHE).

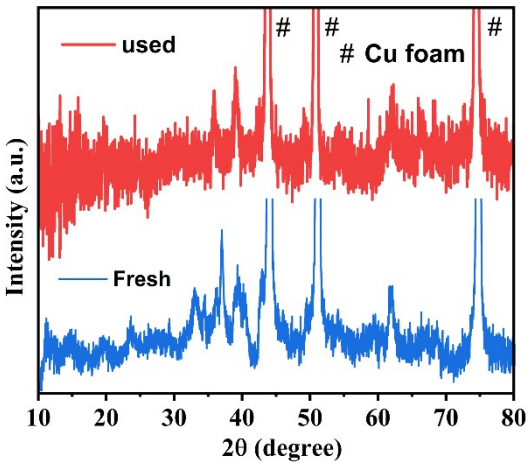

Fig. S15 XRD patterns of fresh and used FeCoNi LDH/CuO/Cu.

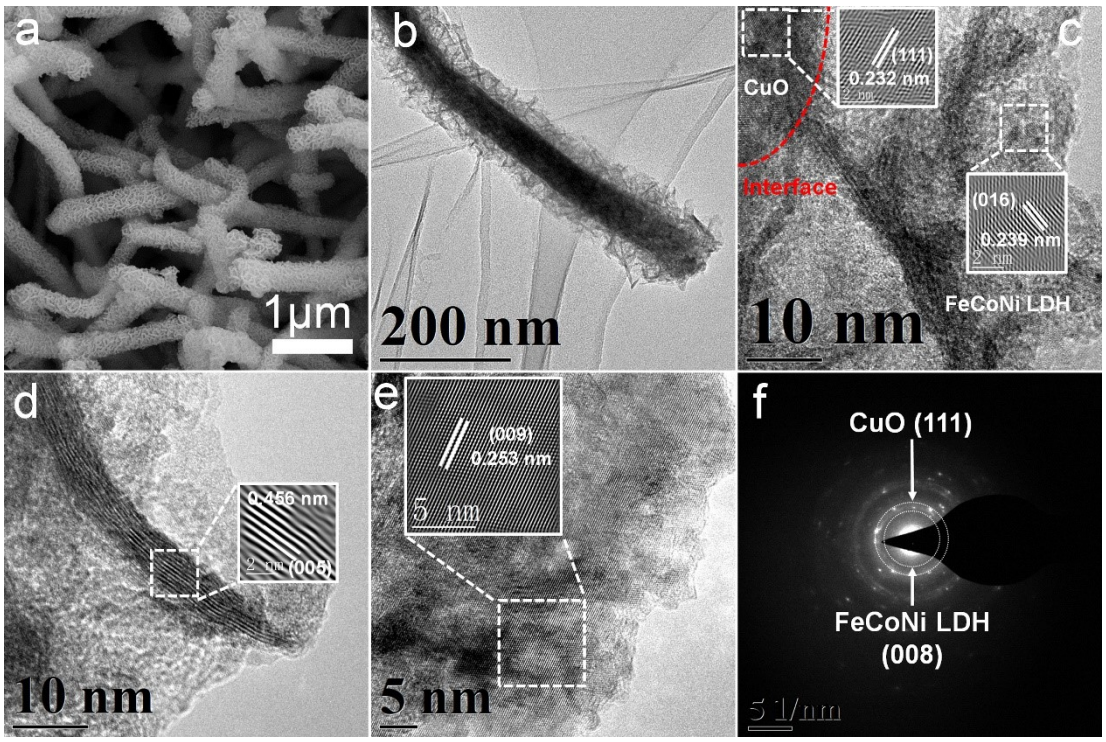

Fig. S16 (a) SEM, (b) TEM, (c-e) HRTEM images, and (f) SAED pattern of the used FeCoNi LDH/CuO/Cu. The inserts in (c-e) are IFFT images corresponding to the regions marked with white dashed boxes.

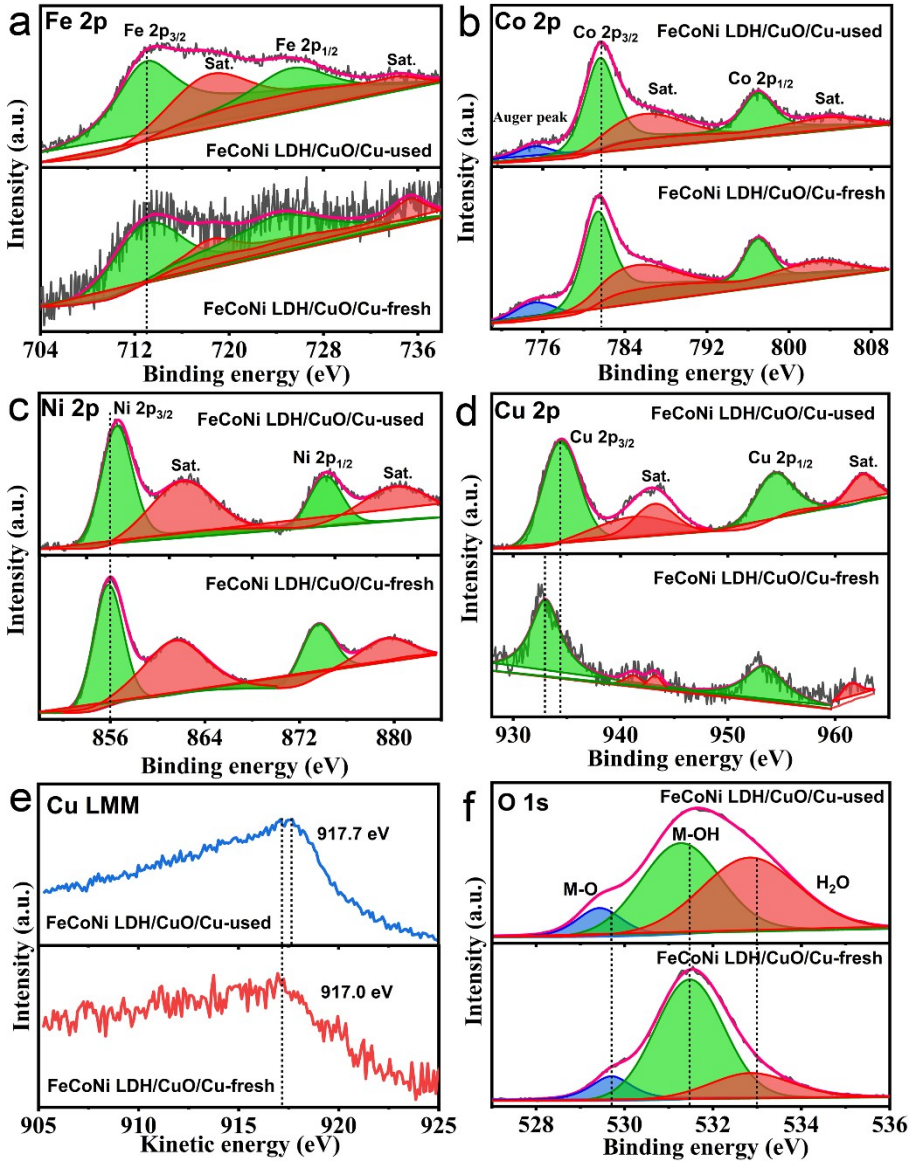

Fig. S17 The high-resolution XPS spectra of (a) Fe 2p, (b) Co 2p, (c) Ni 2p, (d) Cu 2p, (e) Cu LMM, and (f) O 1s of the used FeCoNi LDH/CuO/Cu.

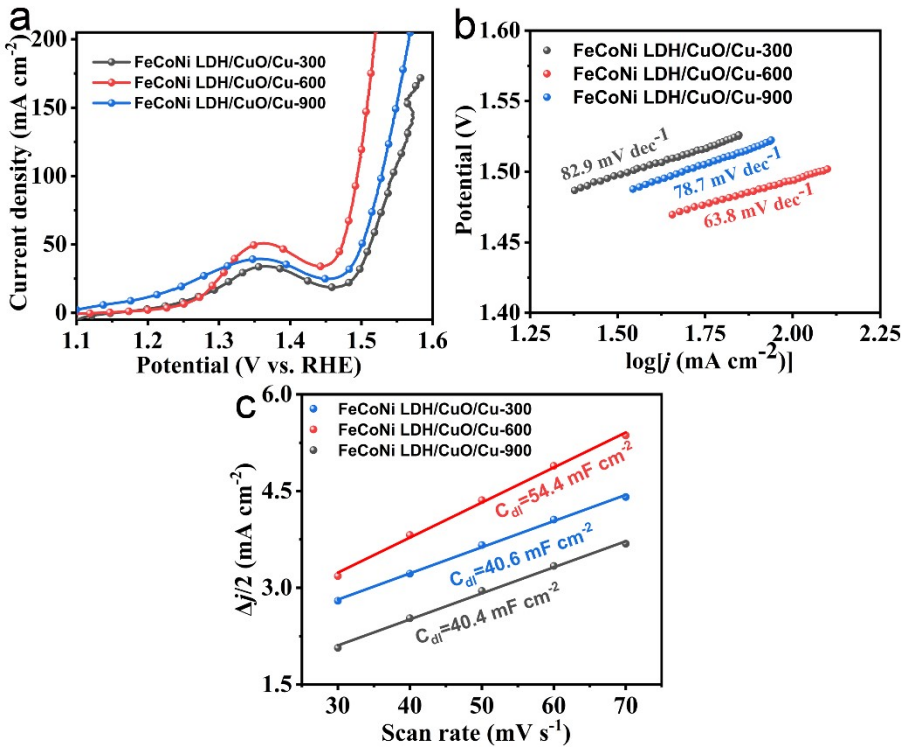

Fig. S18 (a) LSV curves, (b) Tafel slopes, and (c) ECSA

of FeCoNi LDH/CuO/Cu-300/600/900.

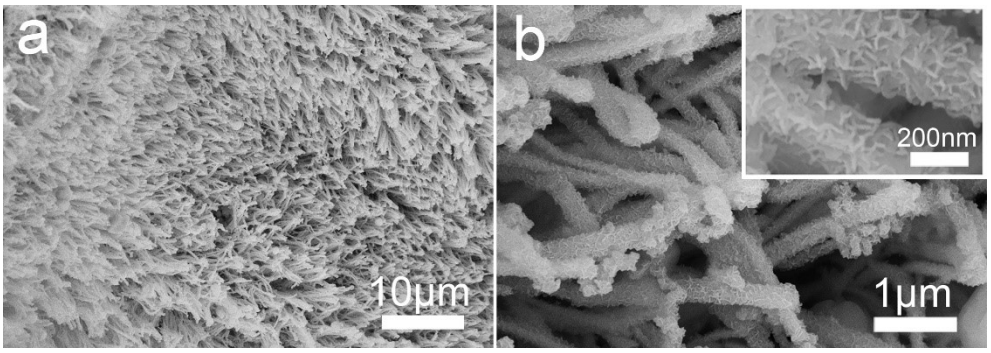

Fig. S19 (a-b) SEM images of FeCoNi LDH/CuO/Cu-300.

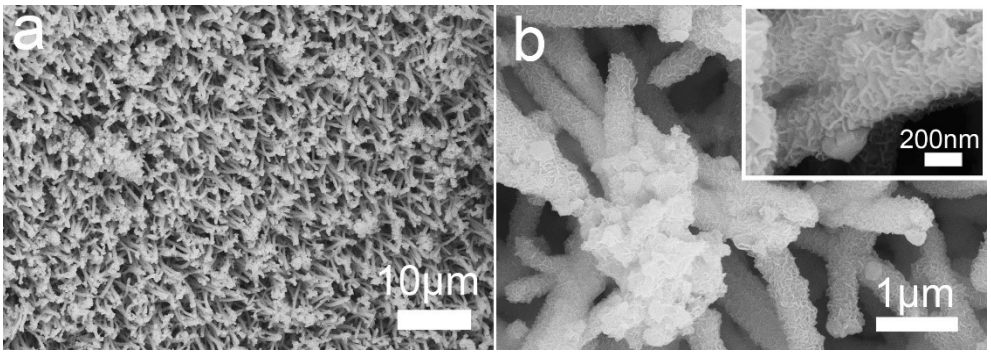

Fig. S20 (a-b) SEM images of FeCoNi LDH/CuO/Cu-900.

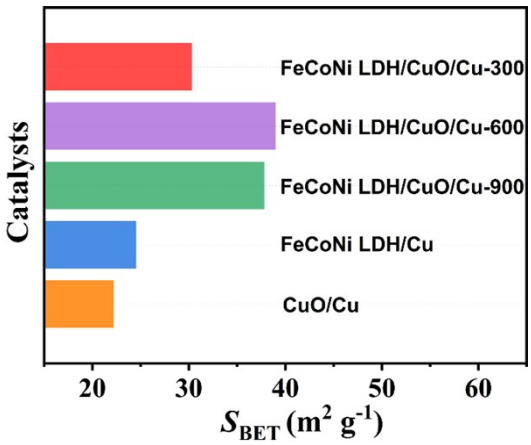

Fig. S21 The BET surfaces of the catalysts.

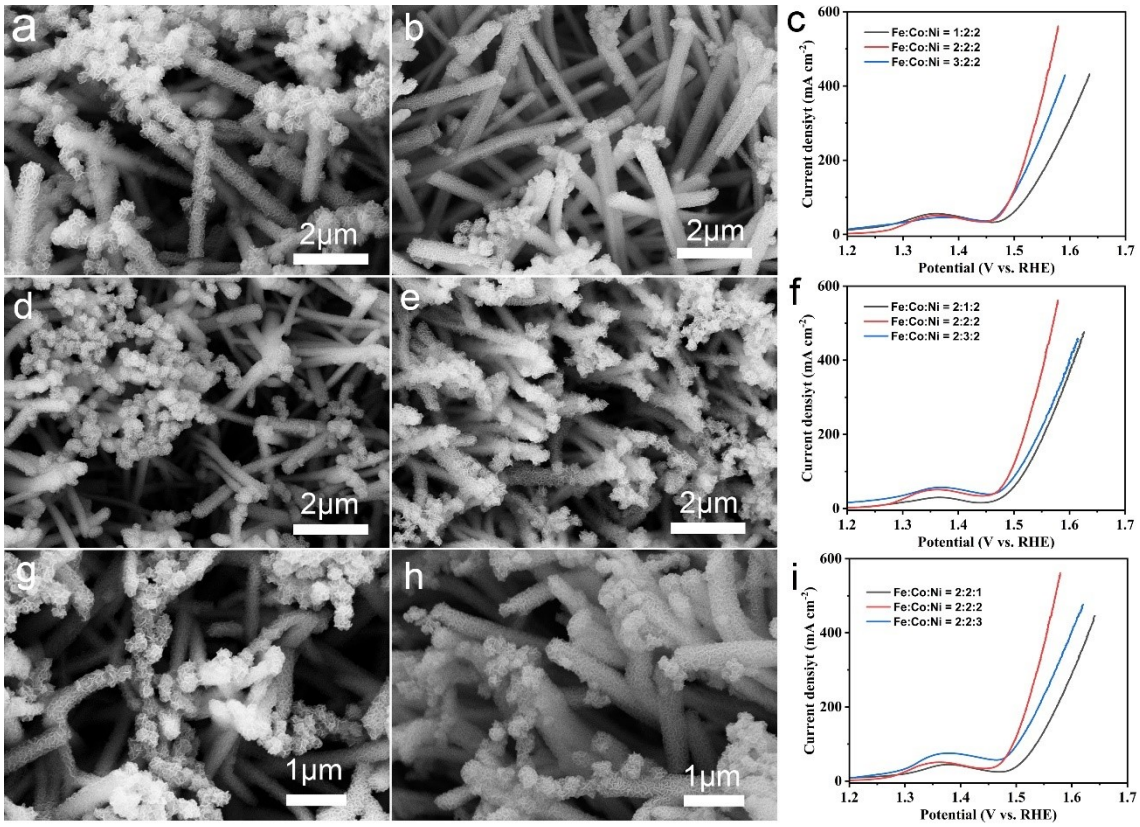

Fig. S22 The SEM images of FeCoNi LDH/CuO/Cu-600s with the different raw materials ratio: (a) Fe: Co: Ni = 1: 2: 2, (b) Fe: Co: Ni = 3: 2: 2, (d) Fe: Co: Ni = 2: 1: 2, (e) Fe: Co: Ni = 2: 3: 2, (g) Fe: Co: Ni = 2: 2: 1, (h) Fe: Co: Ni = 2: 2: 3; LSV curves of the catalysts with (c) different Fe ratio, (f) different Co ratio, and (i) different Ni ratio.

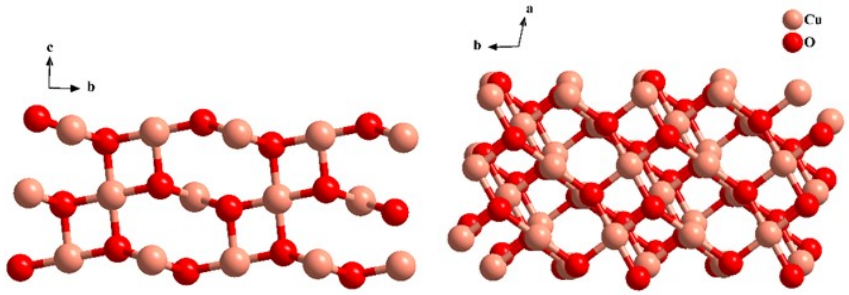

Fig. S23 Side view and top view of CuO.

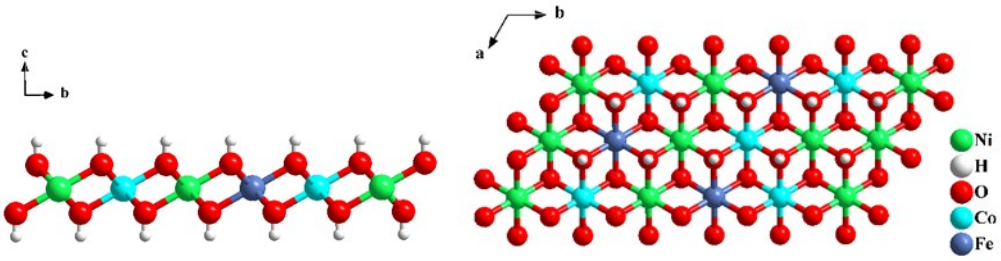

Fig. S24 Side view and top view of FeCoNi LDH.

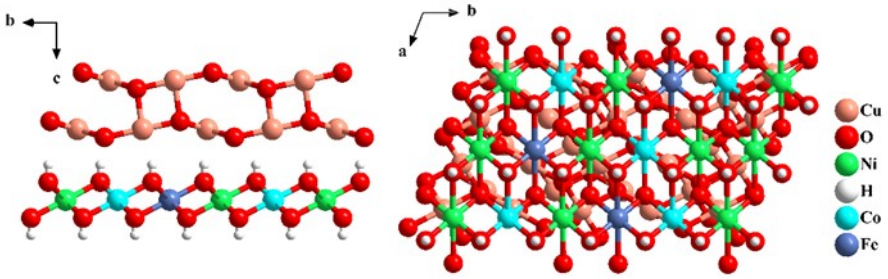

Fig. S25 Side view and top view of CuO/FeCoNi LDH.

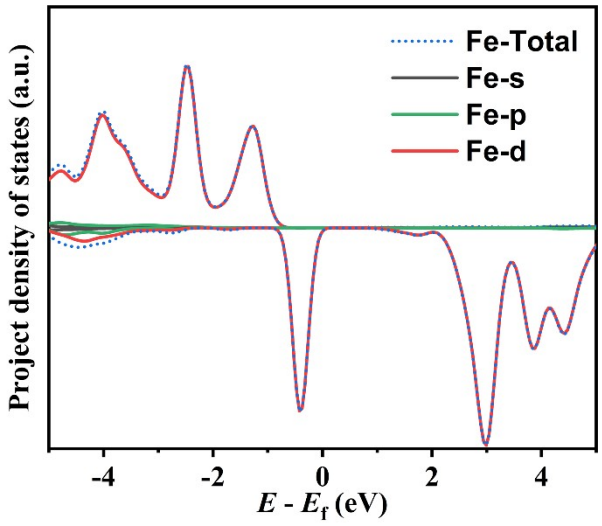

Fig. S26 The PDOS of Fe in FeCoNi LDH.

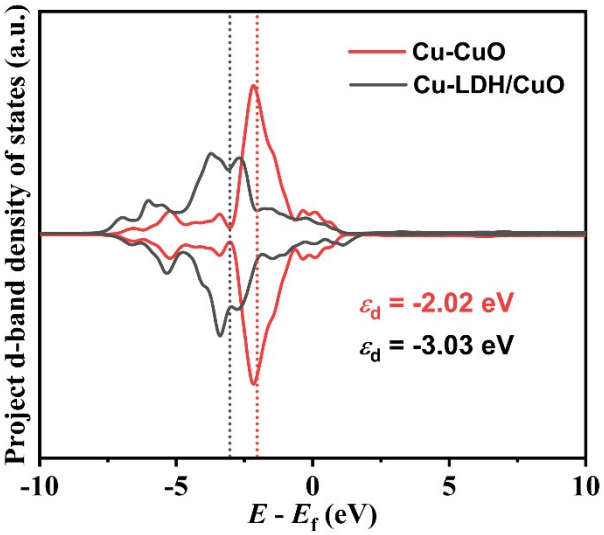

Fig. S27 The PDOS of d orbital of Cu in the catalysts.

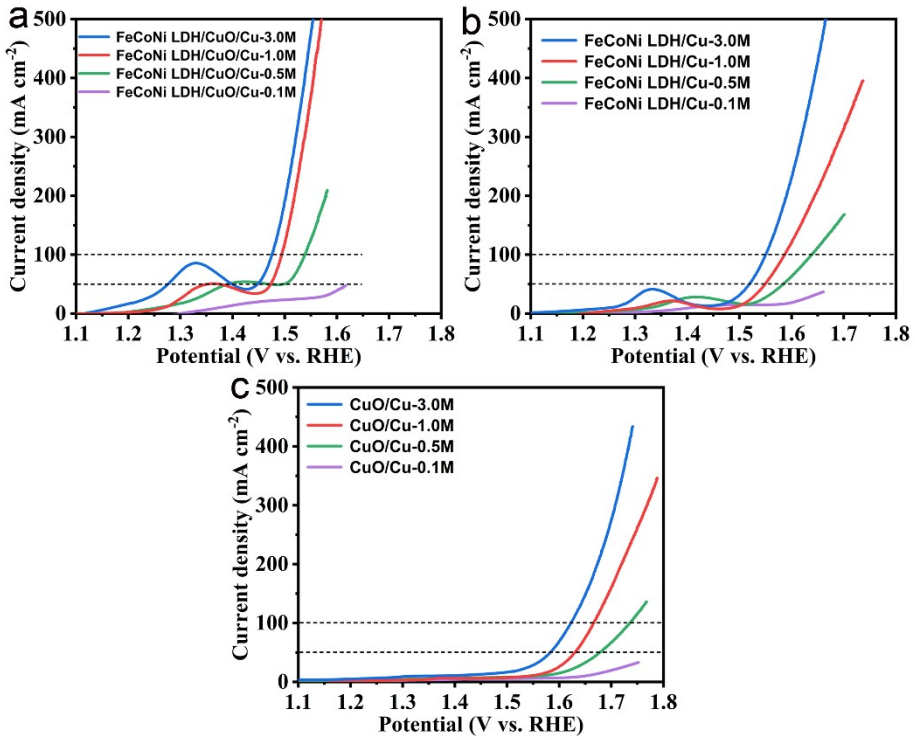

Fig. S28 LSV curves of OER in KOH solution with different concentrations: (a) FeCoNi LDH/CuO/Cu, (b) FeCoNi LDH/Cu, (c) CuO/Cu. The concentrations of KOH solutions are 0.1, 0.5, 1.0, and 3.0 M.

Table S1 The mass loading of catalyst.

Catalysts	Mass loading of CuO/mg	Mass loading of FeCoNi LDH/mg	Total mass loading/mg
CuO/Cu	3.7	--	3.7
FeCoNi LDH/Cu	--	1.6	1.6
FeCoNi LDH+CuO/Cu	3.5	1.7	5.2
FeCoNi LDH/CuO/Cu-300	3.7	0.8	4.5
FeCoNi LDH/CuO/Cu-600	3.7	1.0	4.7
FeCoNi LDH/CuO/Cu-900	3.7	1.1	4.8

*The loading mass of CuO is the difference in mass before and after dissolving CuO on the surface of CuO/Cu in acid. The mass loading of FeCoNi LDH is determined by the mass difference before and after electrodeposition.

Table S2 The element ratio in catalysts obtained by ICP-OES.

Catalysts	Ratio of raw materials/mmol Fe: Co: Ni	Atomic ratio/% Fe: Co: Ni
FeCoNi LDH/Cu	4: 4: 4	20.3: 29.6: 50.1
	2: 4: 4	13.7: 32.6: 53.7
	4: 4: 4	19.9: 30.0: 50.1
	6: 4: 4	29.1: 23.3: 47.7
	4: 2: 4	26.2: 14.2: 59.6
FeCoNi LDH/CuO/Cu	4: 4: 4	19.9: 30.0: 50.1
	4: 6: 4	17.1: 37.4: 45.5
	4: 4: 2	21.1: 36.3: 42.6
	4: 4: 4	19.9: 30.0: 50.1
	4: 4: 6	11.9: 21.2: 66.9

*The results were obtained by scraping the catalyst off the surface of Cu foam and dissolving it in nitric acid and then diluting it at appropriate times.

Table S3 Comparison of OER catalytic performances with other non-noble catalysts.

Catalyst	Current density /mA cm^{-2}	Overpotential vs. RHE/mV	Electrolyte	Tafel slope /mV dec^{-1}	Reference
FeCoNi LDH/CuO/Cu	50 100	243 264	1.0 M KOH	63.8	This work
NiFe-LDH@NiFe-Bi/CC	50	294	1.0 M KOH	96	*Chem. Eur.*, **2017**, 23, 11499-11503
$NiCo_2O_4$@NiFe LDH/NF	50	290	1.0 M KOH	53	*ACS Appl. Mater. Interfaces*, **2017**, 9, 1488-1495
NiFeSe	50	~275	1.0 M KOH	69	*J. Mater. Chem. A*, **2019**, 7, 2831
NiFe LDHs	50	348	1.0 M KOH	67	*Nat. Commun*., **2020**, 11, 2522
NiFeC-SR	50	306	1.0 M KOH	35	*Small*, **2021**, 2101671
Graphdiyne@NiFe LDH composite	10	260	1.0 M KOH	95	*ACS Appl. Mater. Interfaces*, **2019**, 11, 2662-2669
FeCoNi-$NiCo_2O_4$/CC	50	302	1.0 M KOH	71.5	*ACS Appl. Mater. Interfaces*, **2017**, 9, 36917
Ni-Fe LDH hollow nanoprism	10	280	1.0 M KOH	49.4	*Angew. Chem. Int. Ed. Engl*., **2018**, 57, 172-176
CoS_x	10	375	1.0 M KOH	77	*J. Mater. Chem. A*, **2020**, 8, 7647-7652
NiCo LDH nanosheets	10	367	1 M KOH	40	*Nano Lett.*, **2015**, 15, 1421−1427
Cu-Cu_2O/CuO	10	290	1.0 M KOH	64	*Angew. Chem., Int. Ed*., **2017**, 56, 4792
Cu_3P/CuO	10	315	1.0 M KOH	74.8	*ChemElectroChem*, **2018**, 5, 2064
CuO_x @$NiMnO_x$/CF	100	370	1.0 M KOH	80	*J. Mater. Chem. A*, **2020**, 8, 16463-16476
Co_3O_4-CuO Snowflake	20	340	1.0 M KOH	73.3	*J Electroanal Chem.*, **2020**, 871, 114235
CuO NP@G/CF	10	320	1.0 M KOH	63.1	*Chem. Commun.*, **2020**, 56, 8750-8753

Table S4 Bader charge transfer.

Elements	Average charge of atom in pristine models/*e*	Average charge of atom in heterojuntion/*e*	charge transfer/*e*
Fe	-1.34424	-1.45069	-0.10645
Co	-1.22052	-1.26211	-0.04159
Ni	-1.16453	-1.10249	0.06204
Cu	-0.96864	-0.86705	0.10159

* A positive value means that the atom gains electrons and a negative value means that it loses electrons.

Table S5 The potential differences of catalysts to achieve the same current density in different concentrations of KOH solutions.

j/ mA cm^{-2}	Catalysts	*E*(1M KOH)-*E*(3M KOH)	*E*(0.5M KOH)-*E*(1M KOH)
100	FeCoNi LDH/CuO/Cu	18.7	44.1
	FeCoNi LDH/Cu	35.6	52.5
	CuO/Cu	42.7	69.8
50	FeCoNi LDH/CuO/Cu	25.3	24.9
	FeCoNi LDH/Cu	30.4	35.0
	CuO/Cu	48.0	47.3

References

1. C. L. Li, H. Yamahara1, Y. Lee1, H. Tabata1 and J. Delaunay, *Nanotechnology*, 2015, **26**, 305503

2. T. A. Han, J. P. Tu, J. B. Wu, Y. Li and Y. F. Yuan, *J. Electrochem. Soc.*, 2006, **153**, A738.

3. K. Peng, W. Zhang, N. Bhuvanendran, Q. Ma, Q. Xu, L. Xing, L. Khotseng and H. Su, *J Colloid Interface Sci.*, 2021, **598**, 126-135.

4. G. G. Kresse and J. J. Furthmüller, *Phys. Rev., B Condens. Matter*, 1996, **54**, 11169.

5. J. Perdew, K. Burke and M. Ernzerhof, *Phys. Rev. Lett*., 1997, **78**, 1396-1396.

6. Perdew, J.; Burke, K.; Ernzerhof, M. *Phys. Rev. Lett*. 1996, **77**, 3865-3868..

7. Blochl, P. Projector Augmented-Wave Method. *Phys. Rev. B* **1994**, *50*, 17953-17979.

8. S. Grimme, J. Antony, S. Ehrlich and H. Krieg, *J. chem. phys.* 2010, **132 15**, 154104.

9. G. Henkelman, B. P. Uberuaga and H. Jonsson, *J. Chem. Phys.*, 2000, **113**, 9901-9904.